Cell Reports

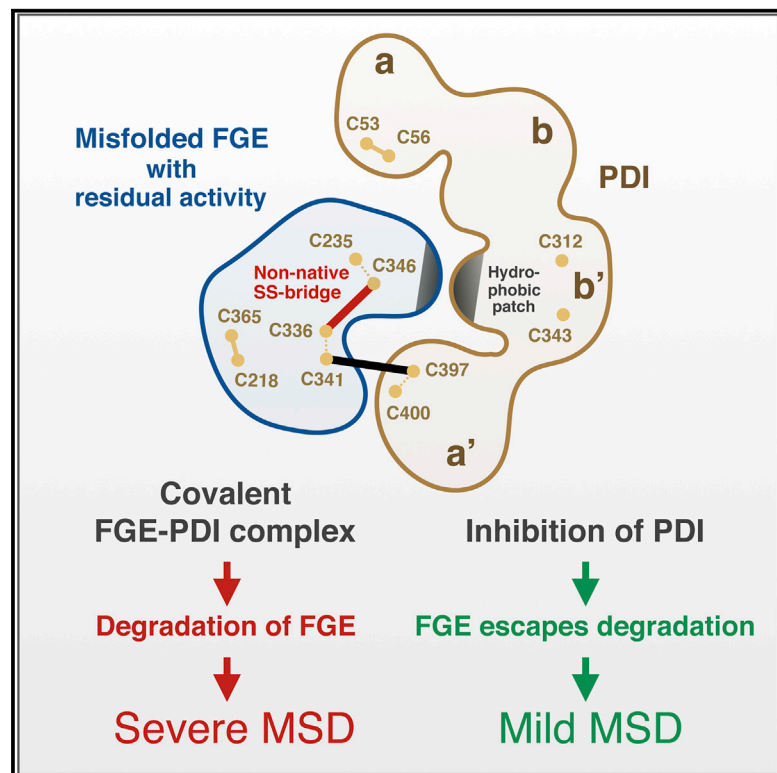# Recognition and ER Quality Control of Misfolded Formylglycine-Generating Enzyme by Protein Disulfide Isomerase

Graphical Abstract

Highlights

- PDI interacts covalently and non-covalently with misfolded FGE

- Non-native disulfide bond in FGE exposes a molecular signature for PDI recognition

- PDI negatively influences misfolded FGE residual activity and intracellular stability

- Inhibition of PDI interaction rescues residual activity of misfolded FGE

Authors

Lars Schlotawa, Michaela Wachs, Olaf Bernhard, Franz J. Mayer, Thomas Dierks, Bernhard Schmidt, Karthikeyan Radhakrishnan

Correspondence

thomas.dierks@uni-bielefeld.de (T.D.), bschmid@gwdg.de (B.S.), kradhak@uni-bielefeld.de (K.R.)

In Brief

Impaired activity of misfolded formylglycine-generating enzyme (FGE) results in multiple sulfatase deficiency (MSD) in humans. Schlotawa et al. show that recognition and quality control of misfolded FGE by protein disulfide isomerase (PDI) play a crucial role in the manifestation of MSD as a severe disease.

CellPress

Recognition and ER Quality Control
of Misfolded Formylglycine-Generating Enzyme
by Protein Disulfide Isomerase

Lars Schlotawa,[1,5] Michaela Wachs,[2] Olaf Bernhard,[3] Franz J. Mayer,[4] Thomas Dierks,[2,6,*] Bernhard Schmidt,[3,*] and Karthikeyan Radhakrishnan[2,3,*]

[1]Department of Medical Genetics, University of Cambridge, Cambridge Institute for Medical Research, Cambridge CB2 0XY, UK
[2]Department of Chemistry, Biochemistry I, Bielefeld University, Universitätsstraße 25, 33615 Bielefeld, Germany
[3]Department of Cellular Biochemistry, University of Göttingen, Humboldtallee 23, 37073 Göttingen, Germany
[4]Bruker Daltonik GmbH, Fahrenheitstraße 4, 28359 Bremen, Germany
[5]Present address: Department of Pediatrics and Adolescent Medicine, University Medical Center Göttingen, Robert-Koch-Straße 40, 37075 Göttingen, Germany
[6]Lead Contact
*Correspondence: thomas.dierks@uni-bielefeld.de (T.D.), bschmid@gwdg.de (B.S.), kradhak@uni-bielefeld.de (K.R.)
 https://doi.org/10.1016/j.celrep.2018.06.016

SUMMARY

Multiple sulfatase deficiency (MSD) is a fatal, inherited lysosomal storage disorder characterized by reduced activities of all sulfatases in patients. Sulfatases require a unique post-translational modification of an active-site cysteine to formylglycine that is catalyzed by the formylglycine-generating enzyme (FGE). FGE mutations that affect intracellular protein stability determine residual enzyme activity and disease severity in MSD patients. Here, we show that protein disulfide isomerase (PDI) plays a pivotal role in the recognition and quality control of MSD-causing FGE variants. Overexpression of PDI reduces the residual activity of unstable FGE variants, whereas inhibition of PDI function rescues the residual activity of sulfatases in MSD fibroblasts. Mass spectrometric analysis of a PDI+FGE variant covalent complex allowed determination of the molecular signature for FGE recognition by PDI. Our findings highlight the role of PDI as a disease modifier in MSD, which may also be relevant for other ER-associated protein folding pathologies.

INTRODUCTION

Multiple sulfatase deficiency (MSD) is a rare but fatal inherited metabolic disorder in humans, characterized by deficient activities of all 17 sulfatases. Sulfatases are activated by post-translational modification of a conserved cysteine in their active site to the catalytic Cα-formylglycine (FGly) residue in the endoplasmic reticulum (ER) (Schmidt et al., 1995; Dierks et al., 1997). The *SUMF1* gene product formylglycine-generating enzyme (FGE) catalyzes this unique modification, and *SUMF1* mutations that impair FGE function were identified as the molecular basis of MSD (Dierks et al., 2003; Cosma et al., 2003). The manifestation of severity in MSD has been attributed to residual functionality of FGE (Schlotawa et al., 2008; 2011). Complete loss of FGE func-

tion is lethal, and it has been suggested that MSD-causing *SUMF1* mutations are hypomorphic, explaining the residual functionality of FGE variants in sulfatase activation (Annunziata et al., 2007). To date, about 40 different MSD-causing *SUMF1* mutations have been reported, and the majority were missense mutations that were predicted to affect the intracellular stability of FGE (Dierks et al., 2005). FGE variants carrying such MSD-causing missense mutations indeed showed clearly detectable activity *in vitro*. In the cell, however, these variants were rapidly degraded, which established that reduced intracellular stability is the major determinant for severity in MSD manifestation (Schlotawa et al., 2011, 2013). Thus, it is of high relevance to understand the basic molecular aspects of misfolding in FGE variants and the mode of recognition by the ER quality control machinery, as holds true for numerous other ER-associated protein folding pathologies.

FGE is a soluble glycoprotein localized in the lumen of the ER. It is also secreted and may even act as a paracrine enzyme (Preusser-Kunze et al., 2005; Zito et al., 2007). The human protein consists of a compact core domain and an N-terminal extension that is proteolytically processed by furin during secretion (Ennemann et al., 2013). The core domain exhibits a novel fold with very low secondary structure content, stabilized by two Ca^{2+} ions and two intra-molecular disulfide bridges (C218/C365 and C235/C346) (Dierks et al., 2005). A pair of conserved redox-active cysteine residues, C336 and C341, which are essential for catalytic activity, line the catalytic site, arranged in a surface-exposed groove of the core domain. FGE uses molecular oxygen for cysteine oxidation, but the precise mechanism is unknown. Structural and functional analyses predicted that FGE could act as a cofactor-less monooxygenase (Dierks et al., 2005; Roeser et al., 2006; Peng et al., 2015), whereas recent data suggest a copper-dependent mechanism (Holder et al., 2015; Knop et al., 2015). The function of FGE has been shown to be a highly regulated process; retention in the ER is promoted by interaction with protein disulfide isomerase (PDI) and ERp44, whereas secretion is facilitated by interaction with ERGIC-53 (Fraldi et al., 2008; Mariappan et al., 2008b). Interestingly, inhibition of exit from the ER upon small interfering RNA (siRNA)-mediated silencing of ERGIC-53 led to proteasomal degradation of
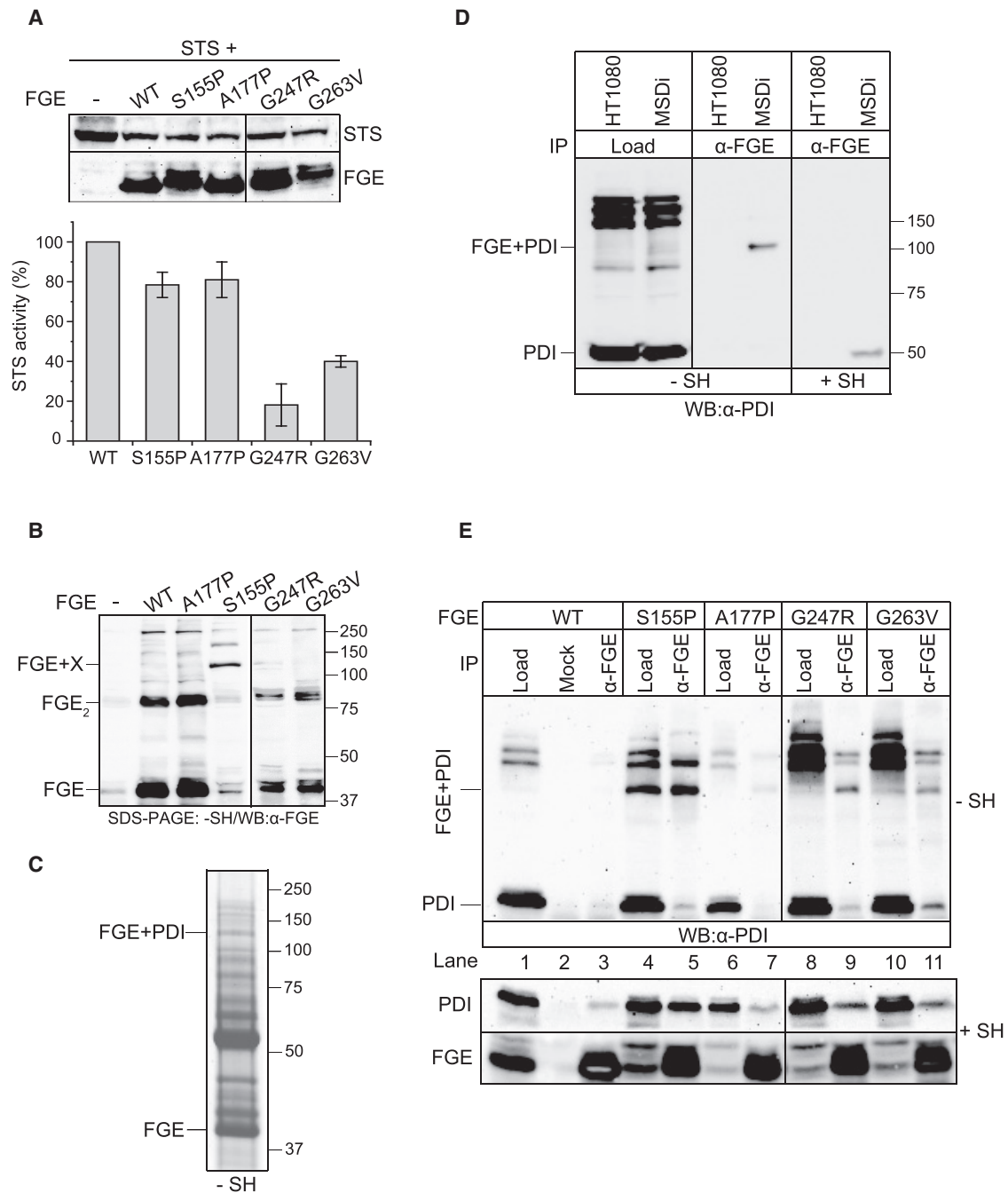
Figure 1. Interaction of PDI with FGE Variants

(A) FGE-mediated activation of STS in MSDi cells. MSDi-TetOn cells were transiently transfected with the indicated combination of cDNAs. The amounts of FGE and STS were monitored by western blotting (top). The measured specific activity of STS from cells coexpressing FGE variants were normalized to that of FGE-WT (100%) and plotted in a bar diagram (bottom). The error bars represent mean ± SEM of values from three independent experiments.

(B) NEM-treated lysates from HT1080 cells stably expressing FGE were resolved in SDS-PAGE under non-reducing conditions and western blot-probed with FGE antiserum.

(C) Identification of PDI in complex with FGE-S155P. HT1080 cells stably expressing C-terminally His-tagged FGE-S155P were treated with NEM, and the lysate was subjected to Ni-NTA chromatography. The elution fractions were resolved in SDS-PAGE under non-reducing conditions, and bands were visualized by Coomassie staining. Excised bands were subjected to in-gel tryptic digestion. Tryptic peptides were analyzed by LC-MALDI mass spectrometry, and the data were used for protein identification in the NCBInr database. The bands with identified monomeric FGE or FGE+PDI are indicated. Results were corroborated by detailed analysis of purified FGE+PDI complex (Figure 3 and Fig. S3A).

FGE, and it was suggested that PDI could function as a cofactor for FGE (Fraldi et al., 2008).

In this study, we demonstrate that PDI plays an essential role in the recognition and quality control of misfolded FGE. Importantly, we show that interfering with this function of PDI rescues sulfatase activities in MSD patient fibroblasts. We were able to purify an *in vivo* covalent complex between PDI and an FGE variant and detect structural determinants underlying the formation of this complex. Our findings provide insight into the molecular pathogenesis of MSD, which is probably also relevant for other protein folding pathologies showing aggravation because of stringent quality control.

RESULTS

PDI Specifically Interacts with Unstable MSD-Causing FGE Variants

To assess the relation between *in vivo* residual activity and stability of FGE variants, we used a well-established steroid sulfatase (STS) *in vivo* reporter assay in immortalized MSD (MSDi) cells, a patient fibroblast cell line with very low endogenous FGE levels (Mariappan et al., 2008a). We chose the stable FGE variant A177P and unstable variants S155P, G247R, and G263V, which cause late infantile mild and late infantile severe forms of MSD, respectively (Schlotawa et al., 2008, 2011). Co-expression of these variants with STS led to comparable amounts of recombinant proteins (Figure 1A). The specific STS activity measured for the different cells revealed that all FGE variants tested showed residual functionality leading to STS activities in the following order: A177P $\geqq$ S155P (75%–85%) > G263V (40%) > G247R (20%) (Figure 1A, with wild-type [WT]-FGE set to 100%). Surprisingly, S155P led to high STS activity, comparable with that of A177P, although the S155P mutation leads to a severe form of MSD in patients.

Cells stably expressing those FGE variants were treated with N-ethylmaleimide (NEM) to block disulfide shuffling and analyzed on western blots under non-reducing conditions. Similar to FGE-WT, the FGE variants A177P, G247R, and G263V showed homodimer formation (Figure 1B), mediated through cysteines C50 and C52 (Preusser-Kunze et al., 2005). In contrast, FGE-S155P showed a prominent band of ~120 kDa (Figure 1B, FGE+X) that was also faintly visible for the other FGE variants. Note that the amounts of monomeric and dimeric forms of FGE-S155P are severely reduced compared with all other variants, indicating that a substantial amount of FGE-S155P is trapped in this complex. Under reducing conditions, the FGE+X complex disappeared with a concomitant increase in monomeric FGE, indicating a disulfide-mediated complex between FGE-S155P and an unknown interacting protein (Figure S1A).

To identify the interacting protein(s), we partially purified FGE-S155P from NEM-treated HT1080 cells stably expressing His-tagged FGE-S155P by Nickel-nitrilotriacetic (Ni-NTA) affinity chromatography under strict non-reducing conditions. The Ni-NTA eluate was resolved by SDS-PAGE. Coomassie-stained bands were excised and analyzed by MALDI-TOF/TOF mass spectrometry after tryptic digestion. Analysis of tryptic peptides from the 120-kDa band identified both PDI (encoded by *P4HB*) and FGE, whereas an ~40-kDa band represented monomeric FGE, as indicated in Figure 1C. Co-immunoprecipitation of endogenous PDI as a complex with FGE-S155P ascertained our mass spectrometry results (Figure S1B). To exclude the possibility that the observed interaction was an artifact of FGE overexpression, we attempted to pull down PDI from untransfected HT1080 or MSDi cells; the latter were derived from a homozygous S155P patient. Analyzing anti-FGE immunoprecipitates from these cells clearly showed a covalent interaction of PDI with endogenous FGE-S155P (in MSDi cells) but not with endogenous FGE-WT(Figure 1D), which suggested a preference for misfolded FGE. When we analyzed cells stably expressing FGE-A177P, FGE-G247R, and FGE-G263V along with FGE-WT and FGE-S155P controls, PDI was found to also exhibit covalent interaction with other FGE variants, but less pronounced, demonstrating a clear general preference for misfolded FGE (Figure 1E). Of note, some weak interaction was also detectable with FGE-WT but only under such overexpression conditions. Moreover, weak monomeric PDI signals in the anti-FGE immunoprecipitates indicated significant non-covalent interaction in all cases.

PDI Regulates Unstable and Stable FGE Variants Differentially

Next we examined the functional consequence of interaction between PDI and MSD-causing FGE variants. Using FGE-S155P as an unstable model protein, we analyzed the effect of PDI overexpression on FGE-mediated activation of sulfatases in MSDi-TetOn cells (harboring FGE-S155P as the endogenous variant). Co-transfection with a plasmid encoding STS and a bidirectional promotor-driven plasmid encoding FGE plus myc-tagged PDI allowed for expression of these three proteins under the control of doxycycline (Figure 2A). Specific STS activities measured were normalized to the very low activity resulting from STS activation by endogenous FGE-S155P (Figure 2A, lane 1). As expected, expression of FGE-WT led to a drastic (91-fold) stimulation of STS activity (Figure 2A, lane 4) that was slightly increased further (98-fold) in case of PDI co-expression (Figure 2A, lane 5), in agreement with data published previously (Fraldi et al., 2008). Remarkably, expression of FGE-S155P also strongly (74-fold) stimulated STS (Figure 2A, lane 6), whereas, in this case, PDI-coexpression largely abrogated this stimulating

(D) Co-immunoprecipitation of endogenous PDI along with endogenous FGE-S155P. Endogenous FGE from NEM-treated lysates of either HT1080 cells or an MSD patient cell line expressing FGE-S155P as endogenous protein were immunoprecipitated using rabbit FGE antiserum. 10% of the starting material (Load) and 50% of immunoprecipitation (IP) fractions were resolved in SDS-PAGE and western blot-probed with mouse monoclonal anti-PDI antibody.
(E) Covalent and non-covalent interaction of FGE and PDI. FGE was immunoprecipitated from NEM-treated lysates from HT1080 cells stably expressing FGE, with either rabbit preimmune-serum (mock) or rabbit FGE-antiserum. 10% of the starting material (Load) and 50% of the IP fractions (α-FGE) were resolved under non-reducing conditions (top) or reducing conditions (bottom) and western blot-probed with mouse anti-PDI or anti-FGE.
(A–E) Representative single-gel analyses; vertical lines indicate lane cropping.
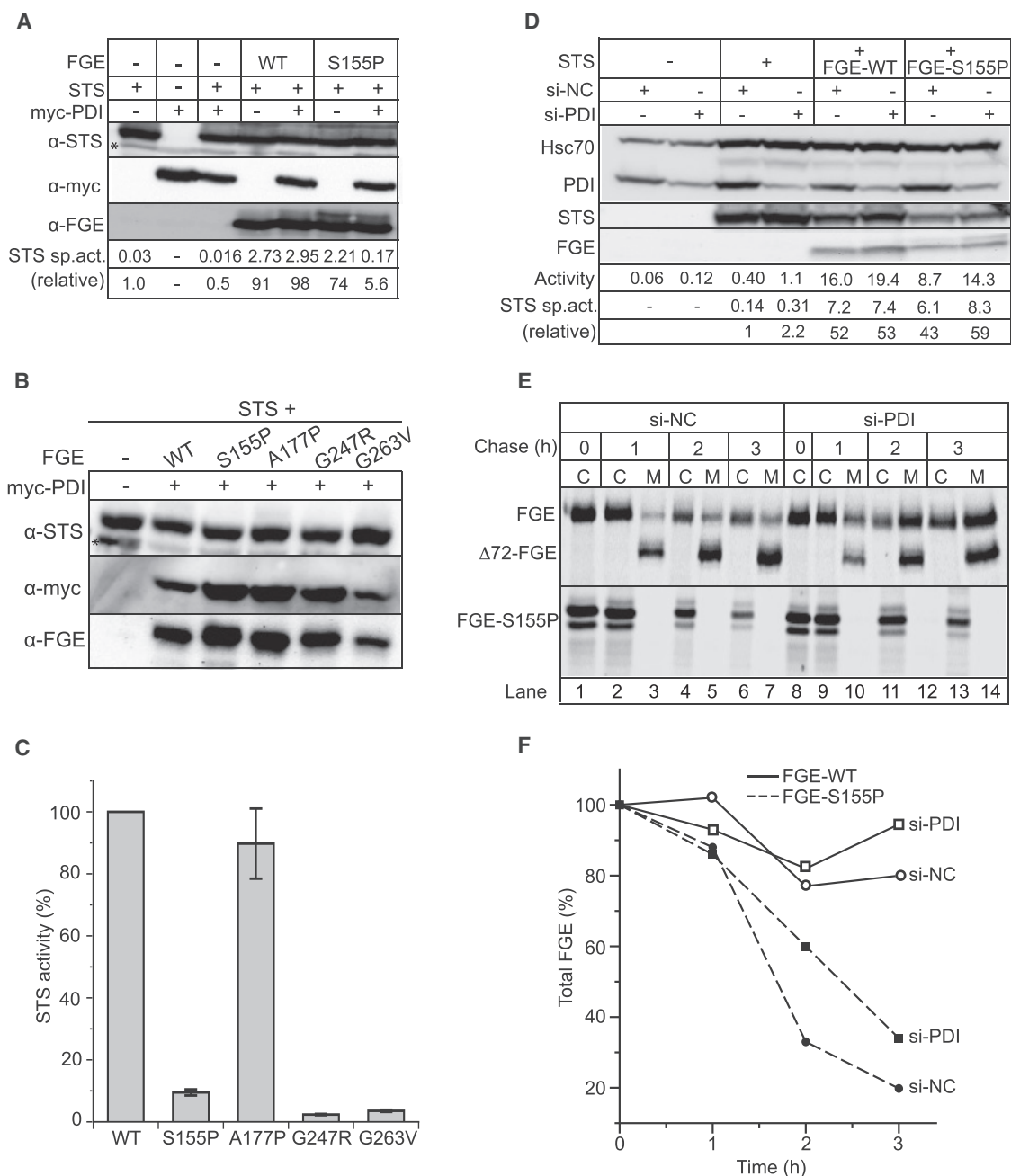
Figure 2. PDI Interferes with FGE-S155P Activity and Stability

(A) Coexpression of PDI impairs FGE-S155P-mediated activation of STS in MSDi cells. MSDi-TetOn cells were transiently transfected with pBI plasmids encoding STS alone, myc-PDI alone, or myc-PDI plus FGE from a bidirectional promoter. STS activity assays were performed from cell lysates. STS-specific activities are presented relative to STS alone-transfected cells (left). The asterisk indicates an unspecific signal.

(B and C) Coexpression of PDI only impairs the activity of unstable FGE variants. STS activity assays were performed in MSDi-TetOn cells coexpressing the indicated proteins, and the amounts of STS, FGE, and myc-PDI were calculated from the western blot (B) (the asterisk indicates an unspecific signal). The measured specific activities of STS from cells coexpressing FGE variants were normalized to that of FGE-WT(100%) and plotted in a bar diagram (C). The error bars represent mean ± SEM of values from three independent experiments.

(D) Inhibition of PDI function by siRNA silencing in MSDi cells increases FGE-mediated STS activation for endogenous FGE-S155P and overexpressed FGE-S155P but not for FGE-WT.

(E and F) Intracellular stability of FGE-S155P under siRNA-mediated silencing of PDI expression. HT1080 cells stably expressing FGE-WT or FGE-S155P treated with PDI siRNA (si-PDI) or control siRNA (si-NC) were metabolically labeled with ^{35}S-methionine/cysteine for 30 min and chased with unlabeled methionine/cysteine for the indicated times. FGE was immunoprecipitated from the cell lysate, and medium and IP fractions were resolved in SDS-PAGE and analyzed by autoradiography (E). The amount of FGE in the cells and medium was quantified and expressed as percentage of total FGE as a function of time (F).
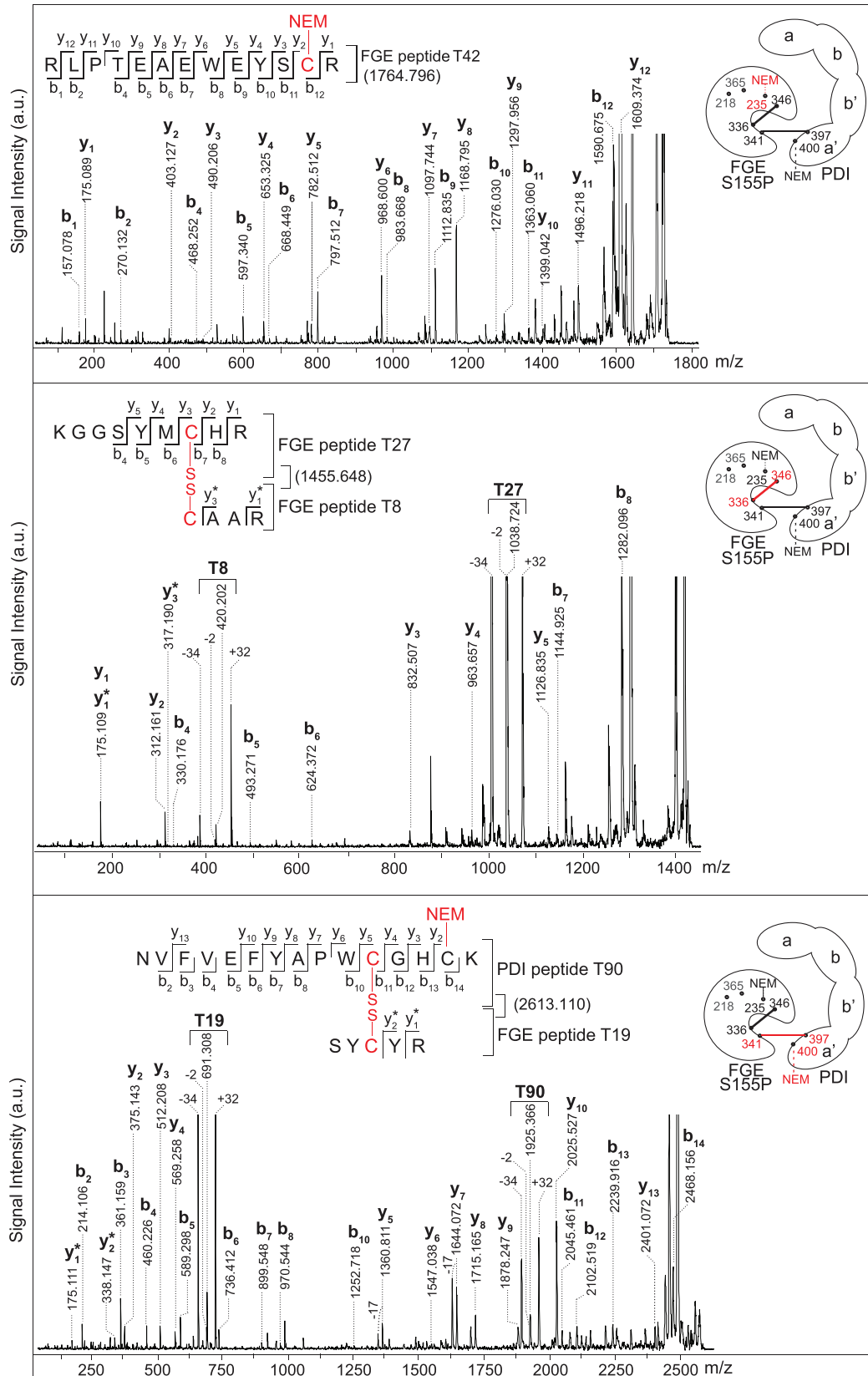
effect (by ≥90%), leaving a residual 5.6-fold increase in STS activity (Figure 2A, lane 7). These data indicate that overexpressed PDI effectively inhibited the residual sulfatase activation function of FGE-S155P. Such an inhibitory effect, albeit only 2-fold, was also observed for endogenous FGE-S155P in cells where PDI alone was expressed along with STS (Figure 2A, compare lanes 1 and 3). When we extended this analysis to other MSD-causing FGE variants, we observed a similar inhibitory role of PDI on the residual activity of the unstable variants G247R and G263V, whereas overexpression of PDI stimulated activity of the stable FGE-A177P variant, leading to an increase (20%–25%) in STS reporter activity to levels observed for FGE-WT co-expression (compare Figures 2B and 2C with Figure 1A).

In a complementary approach, we found that reducing the expression of endogenous PDI stimulated the FGE-S155P mediated activation of STS (Figure 2D). Using siRNA-mediated PDI silencing in MSDi cells, the residual STS activation by endogenous as well as overexpressed FGE-S155P was increased, leading to 2.2- and 1.4-fold stimulation of the STS reporter sulfatase compared with control-oligo (si-NC) treated cells (Figure 2D, compare lane 4 with lane 3 and lane 8 with lane 7, respectively). By contrast, FGE-WT-mediated activation of STS remained unaffected by reduction of PDI expression levels (Figure 2D, compare lane 6 with lane 5). Importantly, PDI knockdown in MSDi cells also led to a 2-fold increase in endogenous sulfatases, as tested for endogenous STS (Figure 2D, compare lane 2 with lane 1) and arylsulfatase A (ASA; Figure S2A) activities, reflecting the rescue of residual FGE-S155P functionality. To verify whether such a rescue can also be achieved by interfering with the *in vivo* interaction between PDI and FGE-S155P, we treated MSDi cells with bacitracin, a membrane-permeable inhibitor of PDI (Figure S2B). A 2- to 3-fold increase in the specific activity of ASA was clearly measurable after 48 hr of treatment.

To verify whether its functional rescue is due to increased intracellular stability of FGE-S155P, we analyzed the fate of FGE-S155P (and FGE-WT as a control) upon PDI knockdown by metabolic pulse-chase analysis (Figures 2E and 2F). Upon overexpression, FGE-WT that escapes the ER retention mechanism is secreted, and the secreted FGE is found in an N-terminally truncated form (Δ72-FGE) because of furin-mediated processing along the secretory pathway (Preusser-Kunze et al., 2005; Ennemann et al., 2013). Interestingly, PDI silencing led to an increase in the proportion of unprocessed FGE-WT in the secreted fraction compared with untreated cells (Figure 2E, top, compare lanes 7 and 14); however, the total amount of FGE remained largely unchanged during the 3-hr chase (Figure 2F). In contrast, FGE-S155P was clearly absent in the secretions, and only ~30% of the intracellularly retained protein was recovered after 2 hr of chase, indicating rapid degradation in

control cells (Figure 2E, compare lanes 1 and 4; Figure 2F). PDI-silenced cells showed a delay in the degradation kinetics, and ~60% of the retained FGE protein was recovered after 2 hr (Figure 2E, compare lanes 8 and 11; Figure 2F). Increased retention of other tested misfolded FGE mutants, but not FGE-WT or FGE-A177P, also suggests that the intracellular stability of mutants G247R and G263V can be rescued by PDI knockdown (Figure S2E). All the above data put together indicate that PDI either positively (for stable FGE-WT and FGE-A177P) or negatively (for unstable FGE-S155P, FGE-G247R, and FGE-G263V) influences the residual activity of FGE.

The S155P Mutation Results in Non-Native Disulfide Configuration in FGE, Leading to Covalent Interaction with the PDI a' Domain

To gain insight into the structural basis of interaction, we purified the FGE-S155P+PDI complex from a stable cell line, co-expressing both proteins, to near homogeneity (Figure S3A). Cells were pre-treated with NEM, and utmost care was taken to prevent artificial disulfide formation and shuffling (STAR Methods). The purified complex was subjected to in-solution tryptic digestion, followed by LC-MALDI-TOF/TOF analysis of cysteine-containing peptides (Figure 3). Except for the FGE C218-containing peptide, for which the mass is beyond the upper detection limit, we could detect all tryptic peptides of PDI and FGE with cysteines either in disulfide-bridged, unmodified (free), or NEM-modified form.

In the FGE-S155P+PDI complex, C235 of FGE (in FGE-WT bridged to C346) was found only reduced or modified with NEM (Figure 3, top). In contrast, C346 formed a new disulfide bridge to active-site C336 (Figure 3, center). In fact, C346 was exclusively found within this new non-native disulfide bond, which blocks the active-site C336 and is indicative of a loss of the native stabilizing disulfide bridge between C235 and C346. C341 of FGE (the native redox partner of C336 in the active site of FGE-WT) was found forming an intermolecular disulfide bridge to C397 in the a' domain of PDI, constituting the covalent interaction between PDI and FGE-S155P (Figure 3, bottom). In the same peptide complex, we could detect PDI C400 modified with NEM. Residue C400 acts as a resolving cysteine to release the substrate from PDI (Gilbert, 2011), which agrees with the presence of C400 as a free, NEM-reactive thiol in the PDI/FGE complex, whereas C397 covalently holds the misfolded FGE substrate. The cysteines C53 and C56 in the a domain of PDI were not involved in intermolecular disulfide formation with FGE-S155P. In fact, as verified by co-immunoprecipitation analysis, comparable amounts of PDI were pulled down as a 120-kDa complex from WT-PDI-, PDI-C53A-, and PDI-C53A/C56A-expressing cells (Figure S3B, lanes 1-7). In contrast, a covalent complex or interaction per se of PDI with FGE-S155P

Figure 3. Analysis of Tryptic Peptides from the Purified FGE-S155P+PDI Complex by MALDI-TOF/TOF Mass Spectrometry

FGE-S155P+PDI complex was purified from MSDi cells stably expressing FGE S155P-His and His-PDI under strictly non-reducing conditions after pretreatment of cells with NEM. The purified complex was digested with trypsin in the presence of iodoacetamide to exclude an attack on disulfide bridges by free thiol groups. Tryptic peptides were analyzed by LC-MALDI mass spectrometry. In the fragment ion spectra, the presence of disulfide bridges in peptide complexes T27+T8 (center) and T90+T19 (bottom) were proved by the occurrence of mass signal quartets (indicated by square brackets) generated by cleavage of the bridge during post-source decay, leaving peptide fragments that contain a cysteine (±0), thioaldehyde (−2), dehydroalanine (−34), or dithiocysteine residue (+32) (according to Schnaible et al., 2002). Labeled are b- and y-ions, and precursor ion masses (m/z) are shown in brackets. The cartoons on the right indicate the positions of cysteines and disulfide bridges or NEM modifications in the FGE-S155P+PDI complex. Identified disulfide bridges and NEM modifications are shown in red.

A

B

C

D
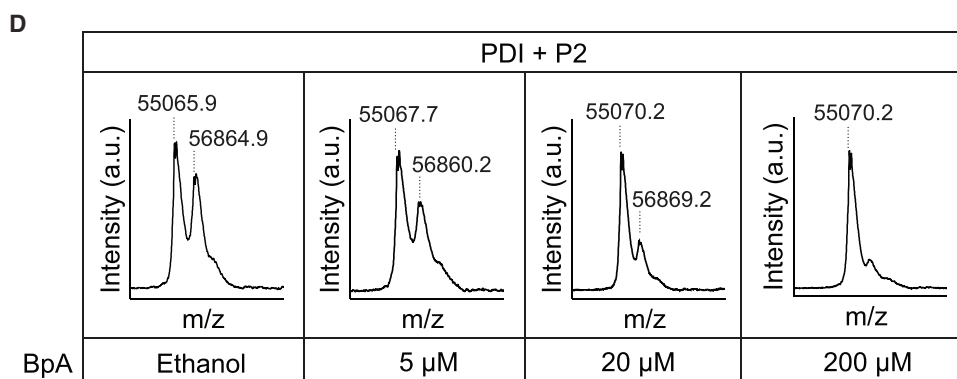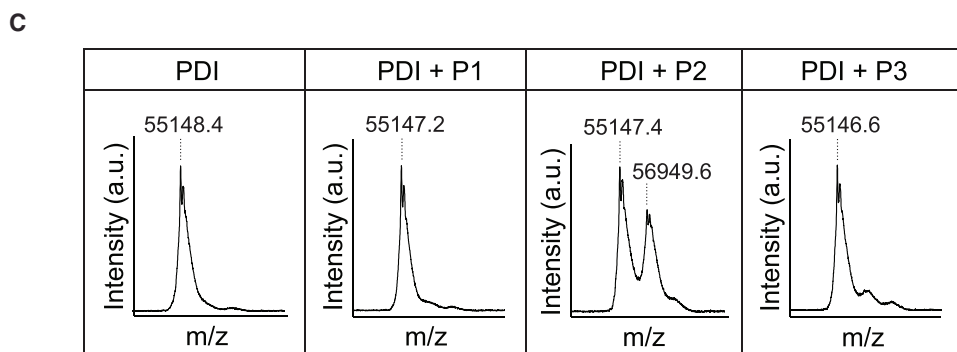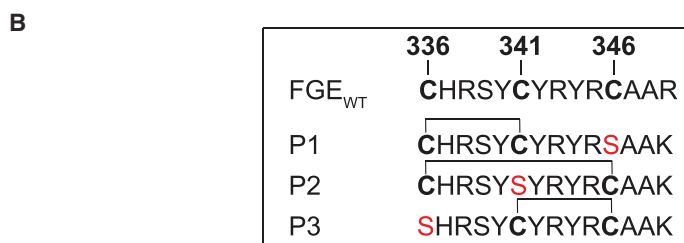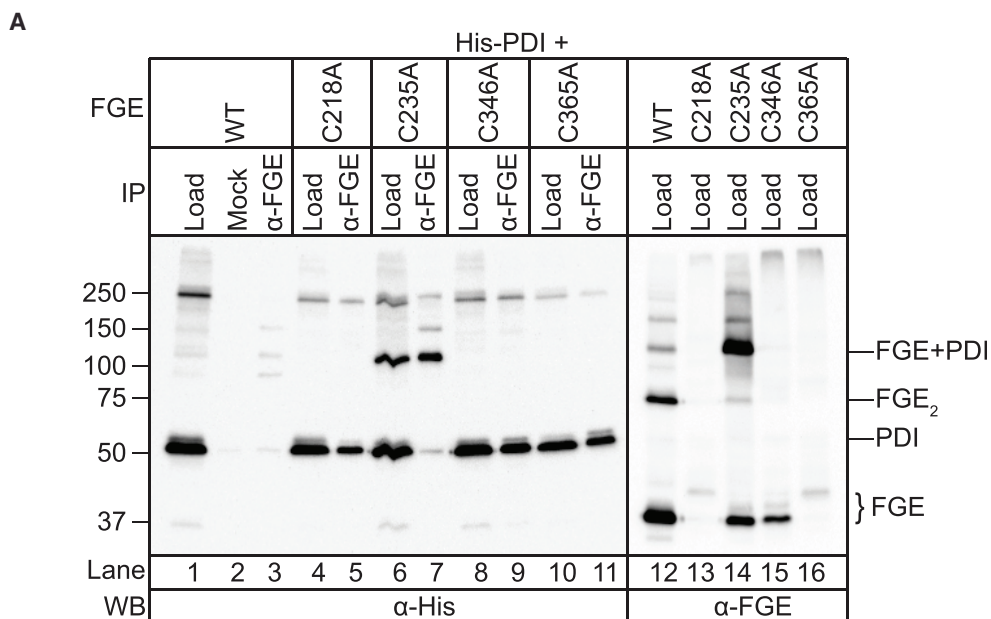
(legend on next page)

was not detectable in either PDI-C397A- or PDI-C397A/C400A-expressing cells (Figure S3B, lanes 8 to 11), suggesting that mutating C397 of the a' domain active site is sufficient to abolish interaction with FGE-S155P, which further substantiates our mass spectrometric data. Of note, mutating the key residues F275 and I289 in a hydrophobic patch of the b' domain of PDI led to a reduction in covalent interaction, suggesting that recognition of exposed hydrophobic residues in FGE-S155P is a prerequisite for covalent interaction (Figure S3C). In fact, earlier studies had shown that PDI mediates hydrophobic interaction with its substrates through this b' hydrophobic patch (Pirneskoski et al., 2004).

Covalent Interaction with PDI Is Determined by a Short Peptide Structure Resulting from Non-native Disulfide Bridging between Cysteines C336 and C346 in FGE

To understand the molecular basis of covalent interaction between misfolded FGE and PDI in further detail, we induced misfolding in FGE by mutating critical cysteines. Two disulfide bridges between cysteine pairs C218-C365 and C235-C346 stabilize the tertiary structure of FGE-WT (Dierks et al., 2005). As expected, all four C/A mutants showed high instability and, different from FGE-WT, were not secreted, indicating destabilization of the structure and failure to pass the intracellular quality control (Figure S4A). Next we analyzed the interaction of these mutants with PDI by co-immunoprecipitation (Figure 4A). We were able to pull down monomeric PDI with FGE-C218A, FGE-C346A, and FGE-C365A, indicating that these mutants interacted non-covalently (Figure 4A, lanes 5, 9, and 11). Interestingly, in cells expressing FGE-C235A, a large fraction of PDI pulled down was found in an ∼120-kDa complex that also contained FGE-C235A (Figure 4A, lanes 7 and 14). The data show that disrupting the native disulfide configuration in FGE results in covalent and non-covalent interactions with PDI. The formation of the covalent 120-kDa complex is exclusively dependent on FGE-C346 that is not disulfide-bonded to its native partner C235. Thus, the covalent intermolecular disulfide bridging of PDI with both FGE-C235A and FGE-S155P (Figure 3, bottom) relies on aberrant FGE intramolecular disulfide bridging involving C346 (Figure 3, center), acting as a molecular determinant for misfolding and PDI-mediated degradation induced by MSD-causing missense mutations like S155P.

To gain insights into the role of C346 in determining the specificity for interaction with PDI, we resorted to *in vitro* analysis of co-

valent interaction between purified recombinant PDI and peptides derived from FGE encompassing cysteine residues C336, C341, and C346, the cysteines involved in the abnormal disulfide bridging leading to the formation of the FGE-S155P+PDI complex. Three peptides with single cysteine mutations (P1, C346S; P2, C341S; and P3, C336S; Figure 4B) were designed, with each containing only two cysteines to result in a defined peptide structure under oxidizing conditions; i.e., upon disulfide bridge formation. The peptides were incubated with bovine PDI in a redox buffer containing varying concentrations of reduced and oxidized glutathione (GSH and GSSG) and, after blocking disulfide shuffling by NEM, analyzed by linear MALDI for complex formation (Figure 4C). Peptide P2, containing C336 and C346, mimicking the disulfide-bridging pattern in the FGE-S155P+PDI heterodimer (Figure 3), efficiently formed a complex with PDI at an oxidizing GSH/GSSG ratio of 1:3. Under the same conditions, peptide P3 showed weak binding, whereas peptide P1, which lacks C346, did not interact. The stability of the PDI+P2 complex under MALDI conditions strongly suggests formation of a covalent bond; i.e., an intermolecular disulfide bridge of PDI with either C336 or C346 of P2. This interaction of P2 with PDI was not observed either under completely oxidizing or completely reducing conditions (Figure S4B), indicating a redox-dependent function of PDI in intermolecular disulfide bond formation. The data clearly show that the cyclic peptide structure stabilized by disulfide bridging of C336 and C346 serves as a molecular determinant for efficient interaction with PDI. Interestingly, when the interaction between PDI and P2 was analyzed in the presence of different concentrations of bisphenol A (BpA), a PDI inhibitor, we observed a BpA dose-dependent decrease in the complex between PDI and P2 (Figure 4D). It has since been shown that BpA inhibits the isomerase activities of PDI by binding to the b' domain (Hashimoto et al., 2012), it is conceivable that PDI, via its isomerase function, acts to resolve the non-native disulfide bridge between C336 and C346 in misfolded FGE.

DISCUSSION

The findings presented in this study show that misfolded FGE is a physiological substrate of PDI and that PDI plays an essential role in MSD by influencing both the stability and the residual activity of MSD-causing FGE variants. Coexpression of PDI severely reduced the residual activity of the unstable FGE variants S155P, G247R, and G263V. By contrast, the stable FGE

Figure 4. The Non-native Disulfide Bridge between C336 and C346 Generates a Molecular Signature for Recognition by PDI

(A) Co-immunoprecipitation of PDI and FGE structural cysteine variants. FGE was immunoprecipitated from NEM-treated lysates from HT1080 cells transiently expressing FGE-WT or the indicated cysteine variants and His-tagged PDI with either rabbit preimmune serum (mock) or rabbit FGE antiserum. 10% of the starting material (Load) and 50% of the IP fractions (α-FGE) were resolved under non-reducing conditions and western blot-probed with mouse anti-His or anti-FGE, as indicated.

(B) Amino acid sequence of synthetic peptides derived from FGE-WT comprising the active-site cysteines C336 and C341 as well as C346. The positions of serines replacing cysteines are indicated in red, and disulfide bridges between the two remaining cysteines are indicated.

(C) Analysis of covalent interaction between the FGE-derived synthetic peptides P1–P3 with bovine PDI in a redox buffer resembling physiological oxidizing conditions by linear MALDI mass spectrometry. Peptide P2, simulating the non-native disulfide bridge found in FGE-S155P, is bound by PDI, as indicated by a mass shift of 1,802 Da in the linear MALDI spectrum, corresponding to the mass of peptide P2.

(D) Bisphenol A inhibits the interaction between P2 and bovine PDI. Peptide P2 and bovine PDI were incubated in the presence of various concentrations of bisphenol A, and complex formation was analyzed by linear MALDI. Analysis with ethanol only served as a carrier control.

Note that linear MALDI analyses, as shown in (C) and (D), were performed on two different instruments. Formation of the P2-complex with PDI in both cases led to a mass increase of 1,799–1,802 m/z, which matches the mass of P2. The average molecular mass calculated for reduced bovine PDI is 55,167 $[M+H]^+$.

variant A177P, predicted to cause MSD because of compromised sulfatase substrate binding (Dierks et al., 2005), was activated by PDI coexpression. We tested whether PDI might play a direct role as a redox partner for FGE's enzymatic activity. However, we did not observe a stimulating effect of PDI on FGE activity in *in vitro* assays performed with purified proteins (Figure S2C). Rather, the data presented in this study agree with the hypothesis that PDI acts as a folding catalyst improving biogenesis of FGE-WT and stable variants, as demonstrated by increasing their *in vivo* activity upon PDI co-expression. Moreover, for instable variants such as FGE-S155P, our data showing that siRNA-mediated silencing of PDI expression led to a decrease in the rate of degradation strongly suggest that the drop in residual activity upon coexpression of PDI is, in fact, due to accelerated degradation. Thus, PDI seems to act as a productive folding catalyst for stable FGE but delivers its substrate to the degradative pathway upon prolonged association with FGE variants with folding problems. As a consequence, for MSD patients, their apparent low FGE residual activity could result, to a large extent, from PDI-mediated accelerated degradation. In line with this, siRNA-mediated silencing of endogenous PDI in the MSDi patient cell line (in which FGE-S155P is the endogenous protein) led to a 2- to 3-fold increase in STS and ASA sulfatase activities, indicating an increase in endogenous FGE-S155P functionality. Considering that the majority of the reported mutations in MSD have been predicted (and many of them shown) to affect the intracellular stability of FGE, our findings strongly suggest that PDI acts as a disease modifier in most MSD patients. Thus, apart from the inherent debilitating effects of these destabilizing missense mutations affecting the activity of FGE, the nature of misfolding and presentation of structural elements for efficient recognition by PDI determine MSD severity.

What are those structural elements recognized by PDI? We also found PDI in a covalent complex with FGE-WT, and coexpression of PDI led to a low but significant increase in the activation of sulfatases, which is consistent with a previous study (Fraldi et al., 2008). Physiologically, PDI obviously catalyzes correct formation of the two stabilizing disulfide bridges (DSBs) in the FGE core domain. It has been suggested that PDI-catalyzed DSB isomerization can occur, while the substrate is in a covalent complex with PDI, by a series of intramolecular disulfide exchange reactions in the substrate. Finally, release of PDI from the substrate is triggered by the attack of a substrate cysteine on the intermolecular DSB (Schwaller et al., 2003). Our data showing that only the C235A mutation led to exclusive trapping of FGE in a covalent complex with PDI suggested that the unavailability of C235 initiates non-native DSB formation of its partner cysteine C346. Most important, our mass spectrometry analysis of the purified FGE-S155P+PDI complex demonstrated that an incorrect DSB between C346 and the catalytic C336 leads to the exposure of C341, another active-site cysteine that is identified by PDI and forms a covalent intermolecular complex. Hence, by analogy with the C235A mutant, it can be inferred that, as a consequence of S155P mutation-induced misfolding, the intramolecular isomerization to resolve the incorrectly formed C336-C346 disulfide in FGE is impaired because of unavailability of C235. In FGE-WT this incorrect DSB could be resolved by C235 to form the

native C235-C346 DSB, and the resulting free C336 could act as a resolving cysteine by attacking the intermolecular disulfide between C341 of FGE and C397 of PDI, thereby releasing PDI. However, the fate of FGE-S155P in complex with PDI is destined for degradation, and it is possible that PDI-C400 could act as a resolving cysteine to release PDI from FGE-S155P. It has been reported that the minimal construct of PDI required for performing DSB isomerization reactions consists of the b' and a' domains (Darby et al., 1998). Our data showing that the covalent interaction of PDI with FGE is dependent only on the b' and a' domain thus indicate that PDI mainly functions as a DSB isomerase to assist FGE with proper folding. b' is known to interact through a hydrophobic patch, as validated here by reduced FGE-S155P binding to the PDI-F275W/I289A mutant. For the substrate side, our finding that the 14-mer FGE peptide P2, exposing a tyrosine-rich sequence upon C346-C336 DSB formation, covalently bound to PDI despite carrying a C341S mutation illustrates that this short sequence determinant is sufficient for firm interaction. Covalent binding of the peptide, however, did not occur under fully oxidizing conditions (GSH:GSSG = 0:100), implicating that, in the absence of C341, PDI has to resolve the artificial C346-C336 DSB to undergo intermolecular DSB formation.

Our data showing that misfolded FGE variants in complex with PDI are destined for degradation identify PDI as an important component of ER-associated protein degradation (ERAD) of misfolded FGE. PDI, through its oxidoreductase and/or chaperone function, is implicated in the ERAD of several misfolded proteins by facilitating their unfolding for subsequent export and degradation in the cytosol (Gillece et al., 1999; Molinari et al., 2002; Lee et al., 2010). Our data suggest that PDI, after attempts to catalyze proper folding, drives terminally misfolded FGE to the degradative pathway. It is known that unfolding of disulfide-containing glycoproteins requires reduction of existing disulfides, and it is possible that PDI could reduce the disulfides and unfold FGE. Interestingly, in a recent study, FGE was identified as an interacting protein with ERdj5 (Oka et al., 2013). ERdj5 is known to interact with mannosidases like EDEM1 and, through its reductase function, has been shown to play an important role in the ERAD pathway. Likewise, PDI has been shown to interact with mannosidase Htm1p to initiate clearance of unfolded glycoproteins from the ER (Gauss et al., 2011). With regard to ERAD of FGE, whether PDI works in co-operation with ERdj5 remains an open question. With regard to MSD, which is an untreatable condition so far, we propose that PDI acts as a disease modifier and could serve as a target for therapeutic intervention.

STAR★METHODS

Detailed methods are provided in the online version of this paper and include the following:

- KEY RESOURCES TABLE
- CONTACT FOR REAGENT AND RESOURCE SHARING
- EXPERIMENTAL MODEL AND SUBJECT DETAILS
  - Cell lines
- METHOD DETAILS
  - DNA constructs
  - Cell culture and transfection

○ PDI RNAi experiments
○ Activity assay for sulfatases
○ Coimmunoprecipitation
○ Metabolic labeling and immunoprecipitation
○ FGES155P-His+HisPDI complex purification
○ Mass spectrometry
○ Insulin-disulfide reduction assay for PDI
○ Peptide binding assays
● QUANTIFICATION AND STATISTICAL ANALYSIS
● DATA AND SOFTWARE AVAILABILITY

SUPPLEMENTAL INFORMATION

Supplemental Information includes four figures and one table and can be found with this article online at https://doi.org/10.1016/j.celrep.2018.06.016.

AUTHOR CONTRIBUTIONS

Conceptualization and Methodology, L.S., B.S., and K.R.; Investigation, L.S., B.S., M.W., O.B., and K.R.; Resources, F.J.M.; Writing-Original Draft and Visualization, K.R.; Writing-Review and Editing, L.S., M.W., B.S., K.R., and T.D.; Supervision and Funding acquisition, B.S. and T.D.

DECLARATION OF INTERESTS

The authors declare no competing interests.

REFERENCES

Annunziata, I., Bouchè, V., Lombardi, A., Settembre, C., and Ballabio, A. (2007). Multiple sulfatase deficiency is due to hypomorphic mutations of the SUMF1 gene. Hum. Mutat. *28*, 928–935.

Conary, J., Nauerth, A., Burns, G., Hasilik, A., and von Figura, K. (1986). Steroid sulfatase. Biosynthesis and processing in normal and mutant fibroblasts. Eur. J. Biochem. *158*, 71–76.

Cosma, M.P., Pepe, S., Annunziata, I., Newbold, R.F., Grompe, M., Parenti, G., and Ballabio, A. (2003). The multiple sulfatase deficiency gene encodes an essential and limiting factor for the activity of sulfatases. Cell *113*, 445–456.

Darby, N.J., Penka, E., and Vincentelli, R. (1998). The multi-domain structure of protein disulfide isomerase is essential for high catalytic efficiency. J. Mol. Biol. *276*, 239–247.

Dierks, T., Schmidt, B., and von Figura, K. (1997). Conversion of cysteine to formylglycine: a protein modification in the endoplasmic reticulum. Proc. Natl. Acad. Sci. USA *94*, 11963–11968.

Dierks, T., Schmidt, B., Borissenko, L.V., Peng, J., Preusser, A., Mariappan, M., and von Figura, K. (2003). Multiple sulfatase deficiency is caused by mutations in the gene encoding the human C(α)-formylglycine generating enzyme. Cell *113*, 435–444.

Dierks, T., Dickmanns, A., Preusser-Kunze, A., Schmidt, B., Mariappan, M., von Figura, K., Ficner, R., and Rudolph, M.G. (2005). Molecular basis for multiple sulfatase deficiency and mechanism for formylglycine generation of the human formylglycine-generating enzyme. Cell *121*, 541–552.

Dimova, K., Kalkhof, S., Pottratz, I., Ihling, C., Rodriguez-Castaneda, F., Liepold, T., Griesinger, C., Brose, N., Sinz, A., and Jahn, O. (2009). Structural insights into the calmodulin-Munc13 interaction obtained by cross-linking and mass spectrometry. Biochemistry *48*, 5908–5921.

Ennemann, E.C., Radhakrishnan, K., Mariappan, M., Wachs, M., Pringle, T.H., Schmidt, B., and Dierks, T. (2013). Proprotein convertases process and thereby inactivate formylglycine-generating enzyme. J. Biol. Chem. *288*, 5828–5839.

Fraldi, A., Zito, E., Annunziata, F., Lombardi, A., Cozzolino, M., Monti, M., Spampanato, C., Ballabio, A., Pucci, P., Sitia, R., and Cosma, M.P. (2008). Multistep, sequential control of the trafficking and function of the multiple sulfatase deficiency gene product, SUMF1 by PDI, ERGIC-53 and ERp44. Hum. Mol. Genet. *17*, 2610–2621.

Gauss, R., Kanehara, K., Carvalho, P., Ng, D.T., and Aebi, M. (2011). A complex of Pdi1p and the mannosidase Htm1p initiates clearance of unfolded glycoproteins from the endoplasmic reticulum. Mol. Cell *42*, 782–793.

Gieselmann, V., Schmidt, B., and von Figura, K. (1992). In vitro mutagenesis of potential N-glycosylation sites of arylsulfatase A. Effects on glycosylation, phosphorylation, and intracellular sorting. J. Biol. Chem. *267*, 13262–13266.

Gilbert, H.F. (2011). Protein Disulfide Isomerases. eLS. Published online April, 2011. https://doi.org/10.1002/9780470015902.a0003021.pub2.

Gillece, P., Luz, J.M., Lennarz, W.J., de La Cruz, F.J., and Römisch, K. (1999). Export of a cysteine-free misfolded secretory protein from the endoplasmic reticulum for degradation requires interaction with protein disulfide isomerase. J. Cell Biol. *147*, 1443–1456.

Hashimoto, S., Shiomoto, K., Okada, K., and Imaoka, S. (2012). The binding site of bisphenol A to protein disulphide isomerase. J. Biochem. *151*, 35–45.

Holder, P.G., Jones, L.C., Drake, P.M., Barfield, R.M., Bañas, S., de Hart, G.W., Baker, J., and Rabuka, D. (2015). Reconstitution of Formylglycine-generating Enzyme with Copper(II) for Aldehyde Tag Conversion. J. Biol. Chem. *290*, 15730–15745.

Knop, M., Engi, P., Lemnaru, R., and Seebeck, F.P. (2015). In vitro reconstitution of formylglycine-generating enzymes requires copper(I). ChemBioChem *16*, 2147–2150.

Lee, S.O., Cho, K., Cho, S., Kim, I., Oh, C., and Ahn, K. (2010). Protein disulphide isomerase is required for signal peptide peptidase-mediated protein degradation. EMBO J. *29*, 363–375.

Lundström, J., and Holmgren, A. (1990). Protein disulfide-isomerase is a substrate for thioredoxin reductase and has thioredoxin-like activity. J. Biol. Chem. *265*, 9114–9120.

Mariappan, M., Gande, S.L., Radhakrishnan, K., Schmidt, B., Dierks, T., and von Figura, K. (2008a). The non-catalytic N-terminal extension of formylglycine-generating enzyme is required for its biological activity and retention in the endoplasmic reticulum. J. Biol. Chem. *283*, 11556–11564.

Mariappan, M., Radhakrishnan, K., Dierks, T., Schmidt, B., and von Figura, K. (2008b). ERp44 mediates a thiol-independent retention of formylglycine-generating enzyme in the endoplasmic reticulum. J. Biol. Chem. *283*, 6375–6383.

Molinari, M., Galli, C., Piccaluga, V., Pieren, M., and Paganetti, P. (2002). Sequential assistance of molecular chaperones and transient formation of covalent complexes during protein degradation from the ER. J. Cell Biol. *158*, 247–257.

Oka, O.B.V., Pringle, M.A., Schopp, I.M., Braakman, I., and Bulleid, N.J. (2013). ERdj5 is the ER reductase that catalyzes the removal of non-native disulfides and correct folding of the LDL receptor. Mol. Cell *50*, 793–804.

Peng, J., Alam, S., Radhakrishnan, K., Mariappan, M., Rudolph, M.G., May, C., Dierks, T., von Figura, K., and Schmidt, B. (2015). Eukaryotic formylglycine-generating enzyme catalyses a monooxygenase type of reaction. FEBS J. *282*, 3262–3274.

Pirneskoski, A., Klappa, P., Lobell, M., Williamson, R.A., Byrne, L., Alanen, H.I., Salo, K.E.H., Kivirikko, K.I., Freedman, R.B., and Ruddock, L.W. (2004). Molecular characterization of the principal substrate binding site of the ubiquitous folding catalyst protein disulfide isomerase. J. Biol. Chem. *279*, 10374–10381.

Preusser-Kunze, A., Mariappan, M., Schmidt, B., Gande, S.L., Mutenda, K., Wenzel, D., von Figura, K., and Dierks, T. (2005). Molecular characterization of the human Calpha-formylglycine-generating enzyme. J. Biol. Chem. *280*, 14900–14910.

Roeser, D., Preusser-Kunze, A., Schmidt, B., Gasow, K., Wittmann, J.G., Dierks, T., von Figura, K., and Rudolph, M.G. (2006). A general binding mechanism for all human sulfatases by the formylglycine-generating enzyme. Proc. Natl. Acad. Sci. USA *103*, 81–86.

Schlotawa, L., Steinfeld, R., von Figura, K., Dierks, T., and Gärtner, J. (2008). Molecular analysis of SUMF1 mutations: stability and residual activity of mutant formylglycine-generating enzyme determine disease severity in multiple sulfatase deficiency. Hum. Mutat. *29*, 205.

Schlotawa, L., Ennemann, E.C., Radhakrishnan, K., Schmidt, B., Chakrapani, A., Christen, H.-J., Moser, H., Steinmann, B., Dierks, T., and Gärtner, J. (2011). SUMF1 mutations affecting stability and activity of formylglycine generating enzyme predict clinical outcome in multiple sulfatase deficiency. Eur. J. Hum. Genet. *19*, 253–261.

Schlotawa, L., Radhakrishnan, K., Baumgartner, M., Schmid, R., Schmidt, B., Dierks, T., and Gärtner, J. (2013). Rapid degradation of an active formylglycine generating enzyme variant leads to a late infantile severe form of multiple sulfatase deficiency. Eur. J. Hum. Genet. *21*, 1020–1023.

Schmidt, B., Selmer, T., Ingendoh, A., and von Figura, K. (1995). A novel amino acid modification in sulfatases that is defective in multiple sulfatase deficiency. Cell *82*, 271–278.

Schnaible, V., Wefing, S., Resemann, A., Suckau, D., Bücker, A., Wolf-Kümmeth, S., and Hoffmann, D. (2002). Screening for disulfide bonds in proteins by MALDI in-source decay and LIFT-TOF/TOF-MS. Anal. Chem. *74*, 4980–4988.

Schulz, C., Lytovchenko, O., Melin, J., Chacinska, A., Guiard, B., Neumann, P., Ficner, R., Jahn, O., Schmidt, B., and Rehling, P. (2011). Tim50's presequence receptor domain is essential for signal driven transport across the TIM23 complex. J. Cell Biol. *195*, 643–656.

Schwaller, M.F., Wilkinson, B., and Gilbert, H.F. (2003). Reduction/reoxidation cycles contribute to catalysis of disulfide isomerisation by protein disulfide isomerase. J. Biol. Chem *278*, 7154–7159.

Zito, E., Buono, M., Pepe, S., Settembre, C., Annunziata, I., Surace, E.M., Dierks, T., Monti, M., Cozzolino, M., Pucci, P., et al. (2007). Sulfatase modifying factor 1 trafficking through the cells: from endoplasmic reticulum to the endoplasmic reticulum. EMBO J. *26*, 2443–2453.

STAR★METHODS

KEY RESOURCES TABLE

REAGENT or RESOURCE	SOURCE	IDENTIFIER
Antibodies		
Rabbit polyclonal anti-FGE	Preusser-Kunze et al., 2005	N/A
Rabbit polyclonal anti-STS	Mariappan et al., 2008a	N/A
Rabbit polyclonal anti-ASA	Gieselmann et al., 1992	N/A
Mouse-monoclonal anti-PDI	Abcam	Cat. #ab2792; RRID: AB_303304
Rat-monoclonal anti-Hsc70	Abcam	Cat. #ab19136; RRID:AB_444764
Mouse-monoclonal anti-RGS-His	QIAGEN	Cat. #34650; RRID:AB_2687898
Mouse-monoclonal anti-c-Myc	Santa Cruz Biotechnology	Cat. #sc-40; RRID:AB_627268
HRP conjugated goat anti-rabbit	Invitrogen	Cat. #31460; RRID:AB_228341
HRP conjugated goat anti-mouse	Invitrogen	Cat. #32430; RRID:AB_1185566
Chemicals, Peptides, and Recombinant Proteins		
N-ethylmaleimide	Thermo Fischer scientific	Cat. #23030
Iodoacetamide	Sigma	Cat. #I1149
BisphenolA	Sigma-Aldrich	Cat. #239658
Bacitracin	Sigma	Cat. #B0125
Doxycycline	ICNbiochemicals Inc.	Cat. #195044
Protease inhibitor cocktail	Sigma	Cat. #P8340
Gluathione, reduced	Sigma-Aldrich	Cat. #G4251
Glutathione, oxidized	Sigma	Cat. #G4626
Trypsin	Serva	Cat. #37283
Protein disulfide isomerase	Sigma	Cat. #P3818
Insulin	Sigma	Cat. #I0516
FGE-peptide P1: CHRSYCYRYRSAAK	This study	N/A
FGE-peptide P2: CHRSYSYRYRCAAK	This study	N/A
FGE-peptide P3: SHRSYCYRYRCAAK	This study	N/A
Deposited Data		
Proteomics	This study	PXD009758
Experimental Models: Cell Lines		
HT1080	ATCC	CCL-121
HT1080-TetOn	Mariappan et al., 2008a	N/A
MSDi	Laboratory of Andrea Ballabio, Italy	N/A
Oligonucleotides		
For PCR-primer sequences, see Table S1	N/A	N/A
siRNA targeting sequence: siPDI-1243: GGACCAUGAGAACAUCGUC	This study	N/A
siRNA targeting sequence: sicontrol-1243: GGACCAUCAGGCCACCUUC	This study	N/A
Recombinant DNA		
pBI-FGE-HA	Mariappan et al., 2008a	N/A
pBI-STS	Mariappan et al., 2008a	N/A
pBI-FGE-A177P-HA	This study	N/A
pBI-FGE-S155P-HA	This study	N/A
pBI-FGE-G247R-HA	This study	N/A
pBI-FGE-G263V-HA	This study	N/A
pBI-FGE-C218A-HA	This study	N/A

Continued

REAGENT or RESOURCE	SOURCE	IDENTIFIER
pBI-FGE-C235A-HA	This study	N/A
pBI-FGE-C346A-HA	This study	N/A
pBI-FGE-C365A-HA	This study	N/A
pBI-RGSHis-PDI	This study	N/A
pBI-Myc-PDI	This study	N/A
pBI-FGE-HA-Myc-PDI	This study	N/A
pBI-FGE-S155P-HA-Myc-PDI-C53A	This study	N/A
pBI-FGE-S155P-HA-Myc-PDI-C53AC56A	This study	N/A
pBI-FGE-S155P-HA-Myc-PDI-C397A	This study	N/A
pBI-FGE-S155P-HA-Myc-PDI-C397AC400A	This study	N/A
pBI-FGE-S155P-HA-Myc-PDI- C53AC56A/C397AC400A	This study	N/A
pBI-FGE-S155P-HA-Myc-PDI-F275W/I289A	This study	N/A
pBI-FGE-S155P-HA-Myc-PDI-C312S/C343S	This study	N/A
pSB-FGE-His	This study	N/A
pSB-FGE-S155P-His	This study	N/A
PcDNA3.1-His-PDI	This study	N/A
Software and Algorithms		
Compass for flexSeries 1.4 Part No 269833	Bruker Daltonics Bremen	N/A
flexControl 3.4 (Build 135)	Bruker Daltonics Bremen	N/A
Warp-LC Version 1.3 (Build 136.138)	Bruker Daltonics Bremen	N/A
Proteinscape 3.1.5 474 (Build id: 20140711-1459)	Bruker Daltonics Bremen	N/A
biotools Version 3.2 (Build 6.32)	Bruker Daltonics Bremen	N/A
flexAnalysis Version 3.4 (Build76)	Bruker Daltonics Bremen	N/A
SequenceEditor Bruker Daltonics BioTools 3.2 SR4	Bruker Daltonics Bremen	N/A
Bruker Compass HyStar 3.2-SR 2 (Build 44)	Bruker Daltonics Bremen	N/A
Hyphenation Star PP Version 3.2.44.0	Bruker Daltonics Bremen	N/A
DisulfideDetect Version 1.0.2.2	Bruker Daltonics Bremen	N/A
Other		
Lipofectamine 2000	Thermo Fischer Scientific	Cat. #11668027
Lipofectamine RNAiMAX	Thermo Fischer Scientific	Cat. #13778075
Pansorbin	Calbiochem	Cat. #507861

CONTACT FOR REAGENT AND RESOURCE SHARING

Information and requests should be directed to and will be fulfilled by the Lead Contact, Thomas Dierks (thomas.dierks@uni-bielefeld.de)

EXPERIMENTAL MODEL AND SUBJECT DETAILS

Cell lines

Immortalized fibroblasts from an MSD patient (MSDi) (kindly gifted by Prof. Andrea Ballabio, Naples, Italy) and HT1080 cell lines were maintained at 37°C under 5% CO_2 in Dulbecco's modified Eagle's medium (PAA) containing 10% fetal calf serum (PAN Biotech).

METHOD DETAILS

DNA constructs

The generation of pBI-FGE construct has been described earlier (Mariappan et al., 2008a). Briefly, the cDNA encoding human FGE with a C-terminal HA tag is cloned into the MCSII of pBI vector (Clontech). FGE-cysteine variants were created by site-directed mutagenesis method using pBI-FGE as template and complimentary mutagenesis primers.

The PDIA1 cDNA was synthesized from total RNA, isolated from HeLa cells, by reverse transcription using the Omniscript RT kit (QIAGEN) and an oligo(dT) primer. The first strand cDNA was amplified by PCR with primers PDIA1-NheF and PDIA1-ER5R (Table S1). The PCR fragment was digested with NheI and EcoRV and cloned into MCS I of the pBI vector. Full-length sequencing verified the correctness of the cDNA insert. A c-Myc tag or a RGS-6His tag was inserted after the signal peptide cleavage site by sequential PCR-based reactions: PDIA1-NheF and PDI-mycR or PDI-RGS-6His-R were used for first amplification reaction; PDI-mycF or PDI-RGS-6His-F and PDIA1-ER5R were used for the second. The resulting PCR products were used as templates in an overlapping-extension PCR with primers PDIA1-NheF and PDIA1-ER5R to generate a product coding for myc-tagged or RGS6His-tagged PDI. This product was digested with NheI and EcoRV for cloning into MCS I of pBI vector (for transient expression) or into pcDNA3.1 for stable expression. For coexpression of myc/His-PDI with FGE or its mutants, myc/His-PDI cDNA was cloned into the MCS I of pBI vector that already had wt-FGE or its mutants in the MCS II.

PDI mutants were created by site-directed mutagenesis using respective primers (the coding sequences of specific primers are described in Table S1) using pBI-mycPDI as template. All PCR reactions were performed with Expand High fidelity PCR system (Roche) and the resulting constructs were analyzed by full-length sequencing of coding regions to preclude any PCR-derived errors. The coding sequences of specific primers are described in Table S1.

Cell culture and transfection

Transient transfections were performed with Lipofectamine 2000 as recommended by the manufacturer. 6 h post-transfection, protein expression was induced with medium containing 2 μg/ml doxycycline and 24 h post-induction, the cells and medium were collected for further analysis. MSDi cells were transfected with pSB-FGE-His and pSB-FGES155P-His plasmids and grown in medium containing 800μg/ml genticin (G418 sulfate, Invitrogen). For double expression, FGE cell lines were additionally transfected with the pcDNA3.1HisPDI plasmid and grown in medium with 100 μg/ml hygromycin (Invitrogen). Stable clones were selected and tested for PDI and/or FGE expression by SDS-PAGE and western blotting.

PDI RNAi experiments

The control (siControl-1243: 5′-GGACCAUCAGGCCACCUUC) and PDI-specific siRNA (siPDI-1243: 5′-GGACCAUGAGAACAUC GUC-3′) duplexes were purchased from IBA, Göttingen (Germany). Transfection of siRNA duplexes were performed using Lipofect-amine RNAiMax (Thermo Fischer) as recommended by the supplier. For MSDi-Tet-on cells, the siRNA duplexes were transfected at 50%–60% confluency and after 24 h, the cells were split and after ∼48 h of first transfection, the cells were transfected again with siRNA duplexes and after 8 h, plasmid constructs were transiently transfected. 6 hr after transfection the cells were induced for protein expression with 2 μg/ml doxycycline. After 20 hr of induction, cells and medium were collected and analyzed. For the metabolic labeling (pulse chase) experiments in HT180 cells stably expressing FGE-WT or –S155P, siRNA duplexes transfection was performed as above and 24 h after second transfection, the pulse-chase analysis was performed.

Activity assay for sulfatases

Activity assays of steroid sulfatase (STS) and arylsulfatase A (ASA) were performed as described earlier (Conary et al., 1986). Western blot signals were quantified using the AIDA 2.1 software package (Raytest). Signals of steroid sulfatase are given as relative amounts, i.e., related to signal intensities detected in cells expressing steroid sulfatase only. Relative specific sulfatase activities were calculated, i.e., catalytic activity divided by the western blot signal (arbitrary units) and referred to that of cells expressing the sulfatase only (relative specific sulfatase activity = 1).

Coimmunoprecipitation

Cells were washed with PBS and incubated with PBS containing 20 mM NEM (Sigma) for 5 min at 37°C and harvested. The cell pellets were resuspended in lysis buffer (PBS pH 7,4, 0.5%–1% (v/v) Triton X-100, 20 mM NEM, protease inhibitor cocktail (Sigma)) and lysed by sonication. The cell lysate was centrifuged at 100,000 g for 30 min at 4°C. Equal amounts of protein were incubated either with rabbit preimmune serum or rabbit FGE anti-serum over night at 4°C, followed by incubation with Pansorbin (Calbiochem) for 1 h at 4°C with end-over-end rotation. The Pansorbin pellet was processed according to a protocol described previously (Gieselmann et al., 1992). The pellet was boiled in 1x Laemmli buffer without β-mercaptoethanol. 10% of the starting material prior to immunoprecipitation (load) and 50%–100% of the pellet fraction were subjected to SDS-PAGE either under nonreducing or reducing conditions, transferred to a nitrocellulose membrane for western blotting.

Metabolic labeling and immunoprecipitation

HT1080 cells stably expressing FGE-WT-His or FGE-S155P-His and HT1080 cells transiently expressing FGE-WT or FGE-cysteine variants were grown to near confluency in 3 cm plates. After starving for 1 h in medium depleted of methionine and cysteine, the cells were pulsed with ^{35}S-methionine/cysteine (Hartmann Analytic) for 30 min. Cells and media were collected after incubation for various time points in unlabeled medium. Immunoprecipitation of FGE from cells and media was performed with an FGE polyclonal antiserum according to a protocol described earlier (Gieselmann et al., 1992). Pellets were solubilized in SDS-PAGE loading buffer and subjected to SDS-PAGE and phosphorimaging (BAS 1000, Raytest). Densitometric quantification of FGE was done using the MacBAS software (Fuji).

FGES155P-His+HisPDI complex purification

For the purification of FGE-S155P-His monomer, FGE-S155P-His+His-PDI complex, and His-PDI monomer, MSDi cell lines expressing these proteins were grown to 90%–100% confluence on cell culture dishes. Cells were incubated with 20 mM NEM (Sigma) added to the cell culture medium at 37°C for 5 min prior to scraping off and lysis in lysis buffer (Tris- HCl 20mM, Triton X-100 0.1% (v/v), Protease inhibitor- Mix 1% (v/v), NEM 20mM, pH 7.4). After clearing by centrifugation at 4°C, the samples were loaded on a 1 mL HiTrap column (GE Healthcare) using a ÄKTA Explorer 10S system (GE Healthcare) and washed with buffer I (Tris- HCl 20mM, NaCl 500 mM, Imidazole 60 mM, NEM 20mM, pH 7.4) with a constant flow rate of 1 ml/min. Elution was performed running a 20 to 500 mM Imidazole gradient using elution buffer II (Tris- HCl 20mM, NaCl 500 mM, Imidazole 500 mM, NEM 20mM, pH 7.4) in 20 column volumes at the same flow rate. Selected elution fractions were acidified with TFA (0,1% (v/v)), loaded onto a Reverse Phase C4 column (Jupiter C4, Phenomenex) and washed using buffer A (95% H_2O, 5% acetonitrile, 0.1% TFA) on a SMART system (GE Healthcare). Elution was performed with buffer B (5% H_2O, 95% acetonitrile, 0.1% TFA), running a gradient from 0% to 70% buffer B in 45 min with a flow rate of 100 μl/min. Part of the elution fractions were mixed with Laemmli buffer and analyzed by SDS-PAGE and Coomassie staining under non-reducing conditions thereby monitoring the integrity of the protein complex. The rest of the appropriate fractions were pooled from different identical runs, lyophilized and stored for further analysis.

Mass spectrometry

Purified and lyophilized protein samples (see above) were resuspended in 10 mM Tris-HCl, pH 8 containing 10 mM iodacedamide, incubated for 25 min at 25°C followed by a tryptic digest at 37°C with 1 μg trypsin (Serva). The digestion was stopped by adding TFA to a final concentration of 1% (v/v). Samples were separated, spotted and analyzed by LC-MALDI analysis (EASY-nLC, Proteineer fc II spotter and Ultraflextreme MALDI-TOF/TOF mass spectrometer; Bruker Daltonics, Bremen) following a protocol described before (Schulz et al., 2011). Data analysis was performed using the postprocessing software FlexAnalysis 3.3 (Bruker Daltonics).

Insulin-disulfide reduction assay for PDI

The enzymatic activity of PDI was assessed by a turbidimetric assay for reduction of insulin disulfide (Lundström and Holmgren, 1990). All reagents were freshly prepared on the day of experiment. 500 μl reactions containing 1 mg/ml (0.172 mM) insulin from bovine pancreas (Sigma) in assay buffer (65 mM Sodium Phosphate, pH 7.0, 2 mM EDTA, 1 mM DTT) were incubated at 25°C either in the absence or presence of 15 μg of PDI (Sigma). Measurements for absorbance at 650 nm were performed every 5 min for 30 min.

Peptide binding assays

FGE-derived peptides P1, P2 and P3 were commercially synthesized (JPT Peptide Technologies GmbH, Germany). The sequences are identical to the human FGE amino acid sequence from Cys336 to Arg349 with the exchange of the C-terminal arginine against lysine for improved stability and one of three cysteines exchanged against serine in each peptide (see Figure 4B). The peptides were dissolved in water, incubated in buffer containing 10 mM Tris HCl, pH 8 and 10 mM DTT for complete reduction of cysteines, and acidified with 0.1% TFA. Peptides P2 and P3 were purified on a Luna C18 Reverse Phase HPLC column (Phenomenex) and P1 was purified using a Jupiter C4 Reverse Phase HPLC column (Phenomenex). Purity and redox state of every peptide were assessed by MALDI-TOF/TOF mass spectrometry. Estimation of the amount of purified peptides in 50 mM Tris was done using a Cary 50 spectrophotometer (Varian) at 280 nm in 50 mM Tris HCl. For peptide binding assays, 20 pmol of purified bovine PDI (Sigma) dissolved in 20 mM Tris HCl, pH 8 were incubated with 400 pmol peptide at 37°C in 100 mM Tris HCl, pH 8 containing 10 mM GSH: GSSG with different ratios from 0:1 to 1:0 or after standardization at a ratio of 1:3 GSH: GSSG. The reaction was stopped after 20 min by adding TFA to a final concentration of 1%. The effect of bisphenol A on PDI+P2 interaction was analyzed under the same conditions as described above. The complexes between the peptides and bovine PDI were analyzed by Linear-mode MALDI TOF mass spectrometry and the redox status of the peptides was analyzed by MALDI-TOF/TOF mass spectrometry in the reflectron mode, as described before (Dimova et al., 2009) applying identical laser shots and distribution of shots on every spot following random walk mode. Samples with PDI or peptide alone served as controls.

QUANTIFICATION AND STATISTICAL ANALYSIS

Error bars are represented as mean ± SEM. Statistical analysis was performed with Microsoft Excel. Quantification methods and the value of n is given in the figure legends and Method Details.

DATA AND SOFTWARE AVAILABILITY

The accession number for the mass spectrometry proteomics data reported in this paper is PRIDE: PXD00975.